buildings

MDPI

Article

Effect of Impinging Jet Ventilation System Geometry and Location on Thermal Comfort Achievements and Flow Characteristics

Naif Albelwi [1], Abdullah M.A. Alsharif [2], Abdulrhman Farran [2], H. A. Refaey [2,3,*] and Mohamed A. Karali [4,*]

[1] Department of Architectural Engineering, College of Engineering in Yanbu, Taibah University, Yanbu Al-Bahr 46425, Saudi Arabia
[2] Department of Mechanical Engineering, College of Engineering in Yanbu, Taibah University, Yanbu Al-Bahr 46425, Saudi Arabia
[3] Department of Mechanical Engineering, Faculty of Engineering at Shoubra, Benha University, Cairo 11629, Egypt
[4] Department of Mechanical Engineering, Faculty of Engineering and Technology, Future University in Egypt, New Cairo 11835, Egypt
* Correspondence: mohamedkarali@yahoo.com or mohamed.karali@btu.edu.eg (M.A.K.); hassanein.refaey@feng.bu.edu.eg or hrefaey@taibahu.edu.sa (H.A.R.)

Abstract

Impinging jet ventilation (*IJV*) systems have attracted significant attention due to their potential to augment indoor thermal comfort and airflow distribution. Previous studies have primarily investigated corner and mid-wall *IJV* installations; however, comparative analyses focusing on different diffuser geometries remain limited. Accordingly, this study examines the combined effects of *IJV* diffuser geometry and installation location on thermal comfort indices and airflow characteristics. A full three-dimensional computational fluid dynamics (*CFD*) model, without the use of symmetry, is developed to simulate a realistic office environment ($3 \times 3 \times 2.9$ m^3), operating in cooling mode under hot summer climatic conditions. Three *IJV* diffuser cross-section geometries—triangular, square, and circular—are evaluated at four installation locations (two corners and two mid-wall positions), assuming a fixed occupant location. A combined return and exhaust outlet configuration is adopted. The results indicate that the *IJV* location influences airflow and temperature distributions more strongly than the diffuser geometry. Nevertheless, the circular diffuser exhibits superior performance compared to the triangular and square geometries. The mid-wall location placed behind the occupant and away from the hot exterior wall demonstrates reduced thermal stratification, improved airflow characteristics, and weaker vortex formation, making it the most favorable configuration. From an architectural perspective, these findings highlight the importance of early coordination between ventilation design and office spatial planning, as diffuser placement directly influences occupant comfort zones and furniture layout. Moreover, the preference for mid-wall installations supports a more flexible façade design and allows for greater freedom in organizing workspaces without compromising thermal performance.

Keywords: HVAC; indoor air quality; thermal comfort; impinging jet ventilation; office building; CFD

Academic Editor: Gianpiero Evola

Received: 21 December 2025
Revised: 14 January 2026
Accepted: 28 January 2026
Published: 3 February 2026

1. Introduction

People spend a considerable proportion of their time indoors; therefore, indoor air quality (*IAQ*) is a key factor influencing occupants' health, comfort, and productivity.

Ventilation system design plays a decisive role in determining *IAQ* performance. Ventilation strategies are commonly classified by researchers and practitioners, according to their operational characteristics and application domains. However, achieving both energy-efficient operation and a healthy indoor environment remains a major challenge in ventilation system design. To address these requirements, Karimipanah and Awbi [1] recommended impinging jet ventilation (*IJV*) as a novel ventilation strategy that is suitable for offices, classrooms, and industrial buildings. The fundamental behavior of *IJV* systems was subsequently investigated by Awbi [2], Rohdin and Moshfegh [3], Varodompun [4], and Chen et al. [5].

In an *IJV* system, a high-momentum air jet is supplied at a specific altitude, impinges on the floor, and spreads radially, forming a thin airflow layer that distributes fresh air across the occupied zone. This concept retains the advantages of displacement ventilation (*DV*), also known as sidewall ventilation, while overcoming its primary limitation: low supply momentum. *DV* systems are well known for their high ventilation effectiveness, based on thermal stratification principles [6,7]. In contrast, the higher momentum of the impinging jet enables the supplied air to overcome buoyancy forces generated by internal heat sources, thereby improving air distribution within the working zone.

Chen et al. [8] investigated the influence of supply diffuser geometry on *IJV* performance at a discharge height of 0.6 m under isothermal conditions and demonstrated that diffuser configuration significantly affects near-floor airflow patterns. Varodompun and Navvab [9] further examined the effects of heat load and supply outlet area. Prior studies by Karimipanah and Awbi [1] and Chen et al. [8] reported that jet decline and temperature distribution are moderately influenced by discharge height; however, the impact on *IAQ* and thermal comfort was found to be more substantial. Consequently, discharge heights of approximately 0.4 m above the floor have been widely recommended [10,11].

The airflow and thermal behavior of office spaces equipped with *IJV* under different heat loads were studied by Chen et al. [12]. Their work also evaluated the combined use of *IJV* and chilled ceiling systems, showing that enhanced entrainment reduces temperature stratification. Similarly, Cehlin et al. [13] assessed airflow effectiveness in offices using *IJV* with cooled ceilings, under cooling conditions. Staveckis and Borodinecs [10] analyzed *IJV* performance under various climatic conditions, occupant postures, and diffuser geometries, concluding that *IJV* is suitable for both cooling and heating and provides advanced ventilation efficiency compared to mixing ventilation. More recently, Zhang et al. [14] proposed the application of *IJV* in automotive cabins and demonstrated a significant reduction in suspended coughing droplets, using a physiological thermal comfort model. Duan et al. [15] introduced sinusoidal impinging jet ventilation (*SIJV*), reporting improved thermal comfort and energy efficiency, with energy savings of approximately 7% compared to steady airflow and 52.8% compared to intermittent airflow.

Numerous *CFD* studies have investigated the selection of turbulence models for *IJV* simulations. Commonly used models comprise the standard k–ε, RNG k–ε, realizable k–ε, and SST k–ω models [8,12,16–19], all of which have shown a reasonable predictive capability for impinging jet flow and thermal fields. Based on recent comprehensive reviews by Ameen et al. [20,21] and Yang et al. [22], the RNG k–ε model has been recommended as the most appropriate option due to its superior agreement with the experimental data.

Most existing *IJV* studies have focused on centrally located wall-mounted supply terminals, while corner-mounted configurations have also been widely investigated [20,21,23]. However, detailed investigations addressing the influence of *IJV* installation location on thermal comfort and *IAQ* remain limited. Yamasawa et al. [24] compared center- and corner-mounted *IJV* configurations, reporting improved cooling and ventilation performance for mid-wall installations, although with limited detail. Almohammadi et al. [25] recently

examined the effect of different *IJV* locations on energy performance and thermal comfort in office buildings; however, their analysis was restricted to circular diffuser geometries. Their results indicated that mid-wall *IJV* placement behind the seated occupant and away from the external hot wall minimizes vortex formation in the occupied zone and offers improved comfort and energy-saving potential.

Based on the reviewed literature and to the best of the authors' knowledge, few studies have systematically examined the combined effects of *IJV* diffuser geometry and installation location on airflow characteristics, thermal comfort, and *IAQ*. Therefore, the present study aims to investigate different *IJV* cross-section geometries installed at representative corner and mid-wall locations, using a combined return and exhaust outlet. The outcomes of this work are presumed to provide useful guidance for *HVAC* designers and contribute to the optimization of *IJV* applications in office environments. To further strengthen the originality and novelty of the present work, Table 1 demonstrates the novelty of the present study with comparison to the most related works from the literature. From an architectural perspective, the findings also support informed integration of ventilation components into office layouts, enabling flexible spatial planning without compromising indoor environmental quality.

Table 1. Literature summary and present work novelty.

Ref.	Type of Investigation	*IJV* Location/Geometry	Return/Exhaust Combination	Studying Influence on		
				Thermal Indices	Flow Characteristics	*IAQ*
Yamasawa et al. [24]	CFD/Exp.	Corners–Mid-walls/Circular	Combined	Yes	No	Yes
Ameen et al. [20]	CFD/Exp.	Corners/Triangle–Square–Quadrant	Combined	No	Yes	No
Ameen et al. [21]	CFD/Exp.	Corners/Triangle	Combined	Yes	No	Yes
Almohammadi et al. [25]	CFD/Exp. validation	Corners–Mid-walls/Circular	Separated	Yes	Yes	Yes
Present study	CFD/Exp. validation	Corners–Mid-walls/Circular–Triangle–Square	Combined	Yes	Yes	Yes

Exp.: Experimental and IAQ: indoor air quality.

2. Methods and Setup

2.1. Physical Model

The CFD simulations were conducted for a compact office room with a floor dimension of 3 m × 3 m and a total height of 2.9 m, as shown in Figure 1a,b. The computational domain represents a realistic office environment, containing a single workstation occupied by a seated thermal manikin and equipped with typical furnishings, including a chair, desk, personal computer, and cupboard. Two ceiling-mounted light fixtures were incorporated into the model. One exterior wall includes a glazed window with an area of 1 m^2 and an assumed transmittance coefficient of 0.5, while the remaining internal surfaces, comprising the floor, ceiling, and other walls, are adjacent to conditioned spaces and were therefore assumed to be maintained at steady thermal conditions. All walls were modeled as brick structures with a uniform thickness of 10 cm.

The *IJV* air supply terminal was positioned at a height of 0.4 m above the floor, in accordance with the recommendations reported in the literature [10,11]. Four *IJV* installation locations were considered, taking into account both functional performance and interior layout considerations: two corner positions and two mid-wall positions, relative to a fixed occupant location. These configurations included corner 1 (behind the manikin), corner 2

(in front of the manikin), mid-wall 1 (behind the manikin), and mid-wall 2 (to the right of the manikin). Three diffuser cross-sectional geometries with identical flow areas were evaluated, as depicted in Figure 2: a right triangular section (163 × 163 × 230.5 mm^3), a square section (115 × 115 mm^2), and a circular section with a diameter of 130.08 mm. For the triangular diffuser installed at the mid-wall position, the geometry was oriented such that its hypotenuse faced the room wall to maintain a visually acceptable interior appearance.

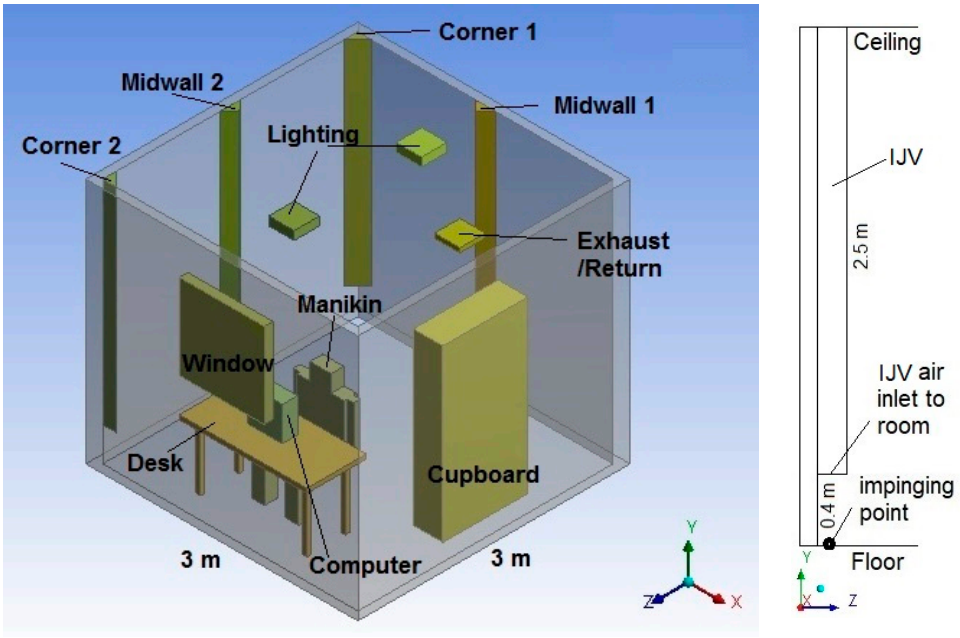

Figure 1. (**a**) Arrangement of the simulated office with an impinging jet ventilation system and (**b**) side view of the *IJV* system, indicating its vertical distance from the floor.

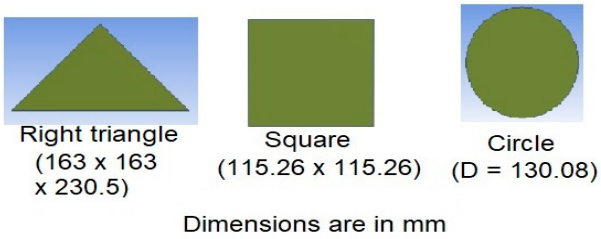

Figure 2. Different *IJV* cross-section geometrical shapes used in the study, from **left** to **right**; right triangle, square, and circle, with dimensions in mm.

The exhaust and return air grilles were combined into a single outlet, located at the center of the ceiling, near the opposite wall, following the configuration reported in [26]. The primary objective of the present *CFD* investigation was to evaluate the combined influence of *IJV* installation location and diffuser cross-sectional geometry on airflow behavior and indoor thermal comfort performance. In total, twelve simulation cases were defined and analyzed, with detailed operating conditions briefed in Table 2.

Table 2. Simulation specifications.

Simulation No.	*IJV* Specifications (Location/Shape)	Simulation No.	*IJV* Specifications (Location/Shape)
1	Corner 1/Triangle	7	Mid-Wall 1/Triangle
2	Corner 1/Square	8	Mid-Wall 1/Square
3	Corner 1/Circle	9	Mid-Wall 1/Circle

Table 2. *Cont.*

Simulation No.	*IJV* Specifications (Location/Shape)	Simulation No.	*IJV* Specifications (Location/Shape)
4	Corner 2/Triangle	10	Mid-Wall 2/Triangle
5	Corner 2/Square	11	Mid-Wall 2/Square
6	Corner 2/Circle	12	Mid-Wall 2/Circle

2.2. Boundary Conditions

The previously investigated office space was evaluated under summer operating conditions that were representative of hot outdoor climates. The external environment was defined by a dry-bulb temperature of 38 °C and a solar heat flux of 700 W/m^2 incident on the exterior façade. Under these conditions, mechanical cooling was required to maintain acceptable indoor thermal comfort. The supply air delivered by the *IJV* system was kept at a constant dry-bulb temperature of 20 °C, with a volumetric flow rate of 75 m^3/h. At the same time, different diffuser locations and cross-sectional geometries were examined, as summarized previously in Table 2.

The selected supply air temperature was determined through a series of preliminary trials based on the specified outdoor conditions and internal heat gains, to achieve an appropriate average operative temperature while minimizing the cooling energy demand. In this study, the target indoor operative temperature was maintained within the range of 24–26 °C at a relative humidity of 50%, in accordance with ASHRAE Standard 55 [27]. The air supply flow rate is set at 75 m^3/h. It is worth confirming that the selected air supply temperature and flow rate typically align with practice in reality for the studied room size and conditions in hot climates. A comprehensive overview of the operating conditions used in the simulations is presented in Table 3. The exterior surface of the wall containing the window was supposed to be maintained at a constant temperature that was representative of outdoor conditions, while the other five internal boundaries, comprising the floor and ceiling, were treated as adiabatic, with no heat transfer to adjacent spaces. Air removal from the room was modeled using a pressure outlet boundary condition set to zero-gauge pressure. The internal heat gains, summarized in Table 4, included contributions from the thermal manikin (125 W), two lighting fixtures (100 W), and a personal computer (60 W), yielding a total internal heat load of 285 W.

Table 3. Room conditions.

Parameter	Values
Air supply temperature	20 °C (dry bulb)
Air supply flow rate	75 m^3/h
Operative temperature	24–26 °C
Relative humidity	50%
Outdoor ambient temperature	38 °C (dry bulb)
Solar heat flux intensity	700 W/m^2

Table 4. Room internal heat loads.

Source of Heat	Heat Load in W
Manikin	125
Lighting	2 × 50
Computer	60
Net	285

2.3. Selection of Turbulence Model and Governing Equations

Guided by recommendations from the reviewed literature on turbulence model selection, this study adopts the Reynolds-averaged Navier–Stokes (RANS) framework, combined with the RNG k–ε two-equation turbulence model. All numerical simulations were carried out using the ANSYS CFX R18.0 solver [28], in which the conservation equations of mass, momentum, and energy were solved to predict the airflow and temperature distributions within the computational domain. Buoyancy effects were accounted for in the momentum equations through the Boussinesq approximation.

The simulations were performed under the assumption of three-dimensional, steady-state, incompressible, and turbulent flow conditions. Detailed formulations of the governing equations and the turbulence modeling approach are available in Karali et al. [29], the ANSYS CFX R18.0 documentation [28], and Ameen et al. [20,30]. Radiative heat transfer was modeled using the discrete transfer radiation model, while pressure–velocity coupling was achieved using the SIMPLE algorithm. Second-order upwind discretization schemes were applied to the pressure, momentum, turbulent kinetic energy, and dissipation of turbulence equations.

Solution convergence was monitored using root-mean-square (RMS) residuals, with convergence thresholds set to 10^{-4} for the energy equation and 10^{-6} for all other variables. To accurately represent the full-scale office environment, all simulations were conducted without imposing symmetry boundary conditions.

2.4. Grid Generation and Independence Validation

In this *CFD* investigation, a non-uniform mesh distribution was generated using ANSYS ICEM CFD R18.0 [28]. Local mesh refinement was applied in regions of high flow gradients, particularly near the air supply inlet, room boundaries, and internal objects. Inflation layers were introduced along solid surfaces to accurately capture near-wall flow behavior, utilizing ten prism layers with an initial layer thickness of 0.08 mm and a growth rate of 1.2. The overall mesh structure of the computational domain is illustrated in Figure 3, including detailed views of the corner *IJV* region and the near-wall boundary layers.

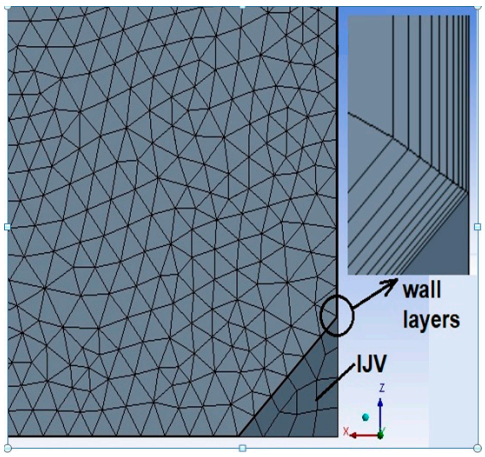

Figure 3. Mesh structure with a zoom-in view for a corner IJV; the **right side** shows another zoom-in view from the wall layers.

A grid independence analysis was conducted to verify an appropriate mesh resolution. Five different mesh densities were generated and evaluated, consisting of 329,316; 1,218,816; 2,042,846; 3,860,062; and 8,814,368 elements. The assessment criterion was based on comparing airflow velocity and temperature profiles measured along a vertical centerline from floor to ceiling within the room. The resulting velocity and temperature distributions for

the tested meshes are presented in Figure 4. Among the evaluated cases, mesh 4 exhibited the smallest deviation relative to finer meshes, while maintaining reasonable computational cost. Consequently, mesh 4, comprising approximately 3.86 million elements, was selected for all subsequent simulations.

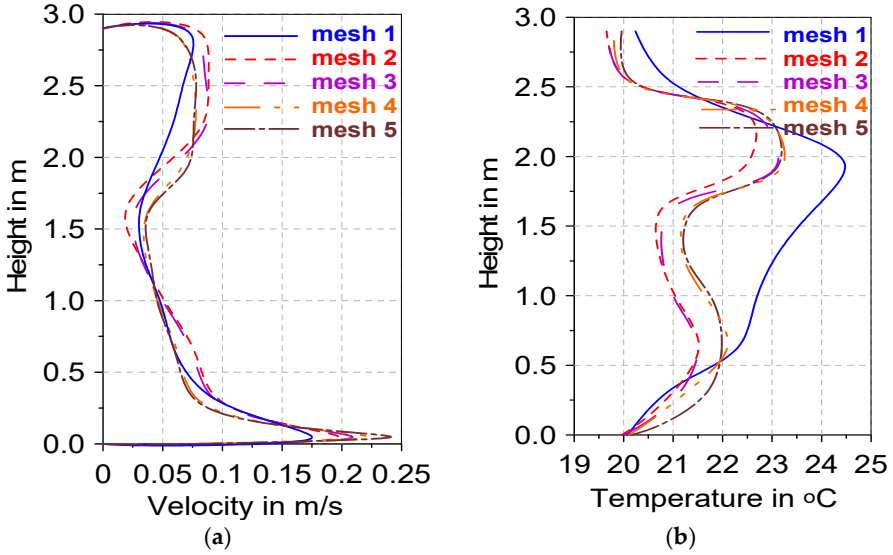

Figure 4. Mesh selection based on the following: measured (**a**) velocities and (**b**) temperature profiles from a vertical centerline inside the room, from floor to ceiling.

2.5. Model Validation with Experiments

The numerical model developed in the present study was first validated against available experimental data reported by Ameen et al. [21]. In their experimental investigation, two triangular *IJV* supply ducts were installed at the room corner, each having an inlet cross-sectional area of 0.0133 m^2 and dimensions of 163 mm × 163 mm × 231 mm. The supplied air temperature was maintained at 17 °C, with an airflow rate of 10 L/s per inlet, resulting in a total supply rate of 20 L/s. The experimental setup assumed an outdoor ambient temperature of 20 °C, while all interior walls were treated as adiabatic. The exhaust outlet was placed at the ceiling near the wall opposite the supply inlets. Thermal manikins representing seated occupants were employed in the experiment, each having a surface area equivalent to that of a human body and generating a metabolic heat output of 100 W. In addition, two enclosures containing halogen lamps were used to simulate internal heat gains, with each lamp producing 75 W, and were placed adjacent to the desks. Model validation was achieved by handling the RNG k–ε turbulence model, and comparisons were conducted at the room centerline, where experimental measurements were available.

However, for further generalization and reliability from the developed CFD model, it is secondly validated with the experimental findings by Yamasawa et al. [24]. As Yamasawa et al. [24] worked on different *IJV* cross-section geometries and locations from those used by Ameen et al. [21]. In Yamasawa et al. [24], two circular *IJV* supply ducts were installed at two mid-wall locations with a diameter of 0.15 m. The supplied air temperature was maintained at 17.5 °C, and the total supply air flow rate was 240 m^3/h, which was assumed to be 100% fresh. The exhaust opening was in the middle of the ceiling. Model validation was performed using the RNG k–ε model, and comparisons were conducted at the room centerline, where experimental measurements were available (point B in Figure 1 [24]). Figure 5(a-1,a-2),b presents a comparison between the experimental data registered by Ameen et al. [21] and Yamasawa et al. [24], respectively, and the numerical predictions obtained from the present *CFD* model. The results demonstrate good agreement between the

simulated and determined temperature and velocity profiles that are available, confirming the consistency of the adopted modeling approach.

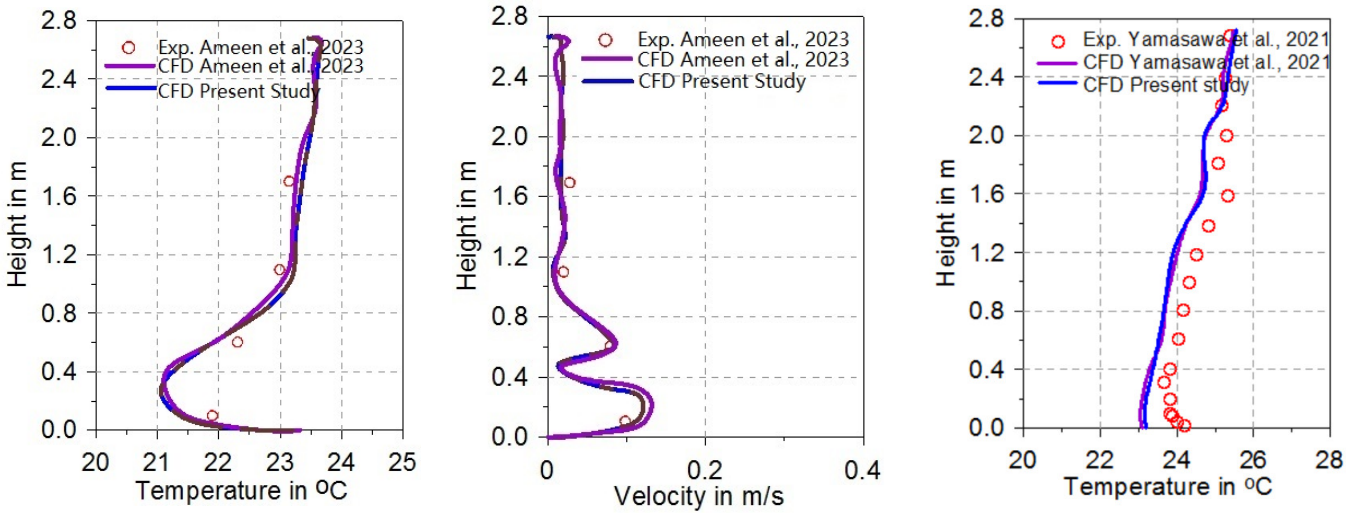

(**a-1**) (**a-2**) (**b**)

Figure 5. CFD model validation with (**a-1**,**a-2**) Ameen et al. [21], and (**b**) Yamasawa et al. [24] experimental results.

3. Quantification of Thermal Comfort Indices

Thermal comfort performance in the present study was quantified using a set of established comfort-related indices, which are described in the following sections. The assessment was concentrated on the local occupied zone, defined as a 1 m^2 area surrounding the seated thermal manikin, representing the primary working region of the occupant. To capture the vertical variations in airflow and temperature within this zone, eleven horizontal sampling planes were defined at heights of 0.1, 0.2, 0.3, 0.4, 0.5, 0.6, 0.7, 0.8, 0.9, 1.0, and 1.1 m above the floor. For each plane, spatially average air temperature and velocity values were extracted from the *CFD* results. These average quantities were then used as representative inputs for calculating all subsequent thermal comfort indices. This approach enabled a detailed evaluation of the vertical distribution of thermal conditions within the occupied zone, ensuring that the computed comfort metrics accurately reflected the thermal environment experienced by the occupant during seated activity.

3.1. Vertical Temperature Difference

The vertical temperature gradient between the head and ankle regions is a significant factor in assessing local thermal comfort. Per ASHRAE Standard 55-2020 [27], the air temperature differential between the ankle level of a seated individual (0.1 m above the floor) and the head level (1.1 m above the floor) must not surpass 3 °C. The vertical temperature gradient is determined using the following equation:

$$\Delta T_{Head-Ankel} = T_{1.1} - T_{0.1} \quad (1)$$

Assessment of this parameter is particularly important due to the natural tendency of air stratification to be associated with impinging jet ventilation systems. In contrast to mixed ventilation systems, which typically produce more uniform temperature distributions, especially during cooling operation, *IJV* systems often generate more pronounced vertical thermal gradients within the occupied zone [31].

3.2. Draught Rate (DR)

The draught rate (*DR*) is another important index used to quantify the level of discomfort experienced by occupants due to unintended local cooling effects. This index estimates the percentage of occupants who are likely to feel dissatisfied due to air drafts. The DR depends on local air velocity, air temperature, and turbulence intensity. Its formulation is provided in ISO 7730-2025 [32] and is also reported in ref. [12].

$$\begin{aligned} &DR = (34 - T) \cdot (u - 0.05)^{0.62} \cdot (3.14 + 0.37 \cdot u \cdot I_l) \\ &For\ u < 0.05\ \mathrm{m/s}\ use\ u = 0.05\ \mathrm{m/s} \\ &For\ DR > 100\%\ take\ DR = 100\% \end{aligned} \quad (2)$$

where T represents the local air temperature, u denotes the mean air velocity, and I—the local turbulence intensity, which can be expressed as follows [12]:

$$I_l = \frac{100(2\,k)^{0.5}}{u} \quad (3)$$

k is turbulent kinetic energy (*TKE*).

ISO 7730-2025 [32] organizes indoor environments, based on *DR*, into three quality categories. Category A corresponds to *DR* < 10%, category B to *DR* < 20%, and category C to *DR* < 30%. In the present study, the draught rate was evaluated at the ankle level (0.1 m above the floor), where occupants are most sensitive to airflow-induced discomfort.

3.3. PMV and PPD

The predicted mean vote (*PMV*) index is a commonly used indicator for assessing the overall thermal comfort in indoor environments. The *PMV* model combines several environmental and personal parameters, including air temperature, mean radiant temperature, air velocity, relative humidity, metabolic rate, and clothing insulation, to estimate the thermal sensation perceived by occupants. According to ASHRAE Standard 55-2020 [27], *PMV* is defined on a numerical scale from −3 (cold) to +3 (hot), where a value of zero represents thermal neutrality, and acceptable thermal comfort is achieved when *PMV* values are close to zero. For seated occupants, *PMV* is typically evaluated at a height of 1.1 m above the floor, corresponding to head level. In the present study, *PMV* calculations were conducted, assuming a metabolic rate of 1.0 MET, which is representative of sedentary office work, and a clothing insulation level of 0.5 CLO, while the relative humidity was maintained at 50% for all simulated cases. In addition, the predicted percentage of dissatisfied (*PPD*) index was used to estimate the proportion of occupants who were likely to experience thermal discomfort due to deviations from neutral conditions. A *PPD* value of 5% corresponds to optimal comfort conditions (*PMV* = 0), while higher *PPD* values indicate increasing levels of thermal dissatisfaction. The *PPD* is calculated as a function of *PMV*, using the following expression [26]:

$$PPD = 100 - 95 \cdot Exp - \left(0.03353 \cdot PMV^4 + 0.2179 \cdot PMV^2\right)\ in\ \% \quad (4)$$

Following the extraction of required inputs, including mean radiant temperature [21], horizontally averaged air temperature and velocity, and the prescribed MET and CLO values, the *PMV* and *PPD* values were determined. *PMV* was computed using the online thermal comfort calculator (Quadco Engineering *PV* [33]), while *PPD* was calculated directly, using Equation (4).

3.4. Mean Age of Air and Air Change Effectiveness

The air quality in an *IJV* is essentially assessed by calculating the average age of the air and measuring the efficacy of air changes (*ACE*). The local average age of air refers to the typical duration it takes for air to travel from the entrance of the supply inlet to a particular position inside the ventilated area. The following is the equation utilized to calculate the average age of air [34,35].

$$\frac{\partial}{\partial x_i}(\rho\, u_i \tau) = \frac{\partial}{\partial x_i} \cdot \left[\left(2.88\, \rho \cdot 10^{-5} + \frac{\mu_{eff}}{Sc_\tau} \right) \cdot \frac{\partial \tau}{\partial x_i} \right] + S_\tau \tag{5}$$

where μ_{eff} denotes the effective turbulent viscosity of air, τ represents the local age of air, and Sc_τ is the turbulent Schmidt number for the age of air, assumed to be 0.7. The source term S_τ was assigned a constant value of 1.0. The air change effectiveness (*ACE*) was utilized to evaluate the efficiency of fresh air distribution within the occupied zone. *ACE* is defined as the ratio of the nominal air exchange time to the mean age of air in the working zone [36]:

$$ACE = \frac{\tau_n}{\tau} \tag{6}$$

where τ and τ_n are expressed in seconds. The nominal time constant τ_n is given by the following:

$$\tau_n = \frac{V_{room}}{q_i} \tag{7}$$

where V_{room} is the volume of the room (m^3) and q_i represents the supply airflow rate (m^3/s). An *ACE* value of 1.0 indicates perfectly mixed indoor air conditioning. According to ASHRAE (1997) [37] and Fan et al. [36], a minimum *ACE* value of 0.95 is recommended to ensure acceptable indoor air quality. Higher *ACE* values indicate more effective ventilation performance and improved *IAQ* within the occupied zone.

4. Results and Discussions

This section presents and discusses the results acquired from the *CFD* simulations conducted in the present study, covering all investigated cases summarized in Table 2. The discussion is structured into two main parts to facilitate a comprehensive evaluation of the system performance. The first part focuses on analyzing thermal comfort indices to identify the *IJV* configurations that best comply with the recommended comfort criteria and relevant standards. These indices are used to assess the suitability of each configuration in providing acceptable thermal conditions within the occupied zone.

The second part examines the airflow behavior and thermal distribution within the room, emphasizing key flow characteristics such as vorticity isosurfaces, airflow streamlines, and temperature contour plots. These visual and quantitative analyses provide deeper insight into the underlying flow mechanisms associated with different *IJV* geometries and installation locations. Together, the combined assessment of thermal comfort performance and flow characteristics supports the final selection of the most effective *IJV* diffuser geometry and placement for office applications.

4.1. Thermal Comfort Indices and Draft Sensation

Figure 6 presents the vertically averaged air temperatures extracted from horizontal planes located between 0.1 m and 1.1 m above the floor within the local occupied zone for all simulated cases. As observed in Figure 6, the corner 1, mid-wall 1, and mid-wall 2 configurations exhibit a clear increase in air temperature with height, indicating the presence of vertical thermal stratification. However, the magnitude of this temperature rise progressively decreases as one moves from the corner 1 configuration to the mid-

wall 1 case and further to the mid-wall 2 configuration, suggesting a gradual reduction in stratification intensity among these setups. This shift in temperature levels continues until an inverted trend is observed for the cases of corner 2. This implies that, under the prescribed conditions, the *IJV* location within the hot wall can invert the typically known thermal stratification for the cooling mode. This means sensing heat at the ankle level more intensely than at the head level. Hence, such behavior can be the first justification for rejecting such *IJV* locations in practice. The second observation from Figure 6 is that the circular cross-section of the *IJV* yields the lowest temperature measurements compared to the other geometrical shapes used: namely, the square and the triangle. It could be noticed from Figure 6 that the temperature increases from a height of 0.1 m to 1.1 m for the case of corner 1–square (simulation 2) from 23.2 °C to 24.7 °C. But for the case of corner 2–square (simulation 5), the temperature decreases from 26.8 °C to 25.5 °C, while very low differences are noticed for most cases of mid-wall 1 and mid-wall 2.

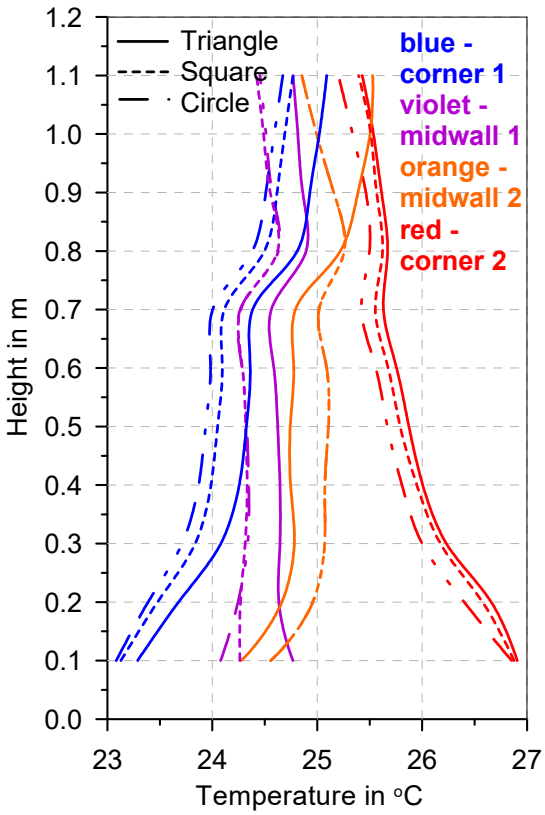

Figure 6. Vertically averaged air temperatures in the local working zone at heights from 0.1 to 1.1 m above the floor for all cases.

The degree of vertical thermal stratification can be further evaluated by calculating the absolute temperature difference between the head and ankle levels (1.1 m and 0.1 m above the floor), as illustrated in Figure 7. The figure also indicates the maximum allowable temperature difference of 3 °C, specified by ASHRAE Standard 55 [27]. The results show that, for all investigated cases, the observed temperature differences remain well below the prescribed limit, with values on the order of approximately 1 °C. These results are consistent with the previously reported findings on temperature stratification that are associated with impinging jet ventilation operating in cooling mode [12,31].

The evaluation of the draught rate (*DR*: Equation (2)) level at ankle level (H = 0.1 m) is illustrated in Figure 8. The results show that the *DR* levels for all studied cases were below the ISO 7730-2025 [32] limits for category A: that is, 10%. The results for corner 1 cases (simulations 1 to 3) showed the highest level of *DR*, with an average value of 9%

(corner 1–square). As expected, the lowest *DR* at the ankle level is recorded for the cases of corner 2 (simulations 4–6), with an average value of 5.7% (corner 2–square). This is due to the relatively hot temperatures found at the ankle level in these cases, which decreases the dissatisfaction caused by cooling.

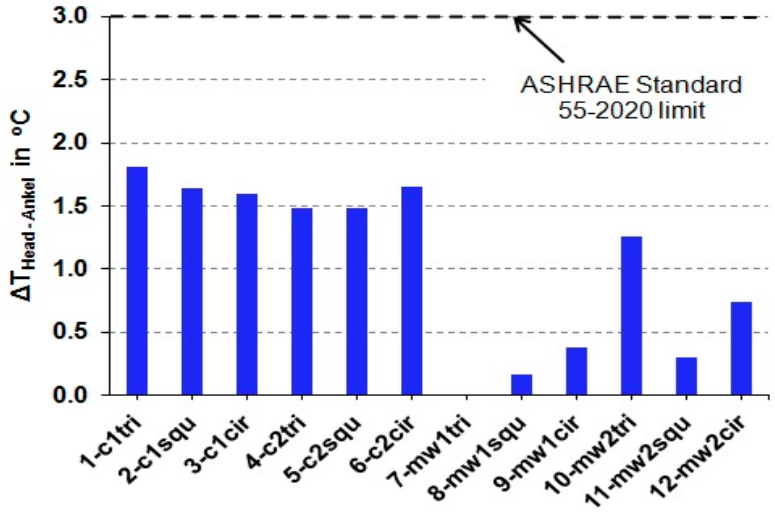

Figure 7. Absolute values of temperature difference among heights 1.1 and 0.1 m within the local comfort zone for all studied cases. c: Corner, mw: mid-wall, tri: triangle, squ: square, and cir: circle. Dashed line is for the ASHRAE Standard 55-2020 limit [27].

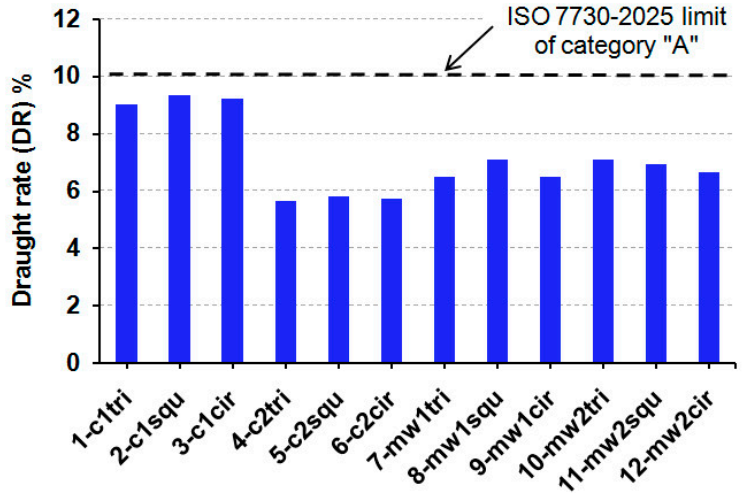

Figure 8. Draught rate (DR) at ankle level (0.1 m above the floor) for all simulated cases. Dashed line is for the ISO 7730-2025 limit [32].

Figure 9 illustrates the variation in the predicted mean vote (*PMV*) along the vertical direction, from 0.1 m to 1.1 m above the floor, for all investigated cases. As shown in the figure, *PMV* values across all configurations fall within a range of approximately −0.32 to 0.53. According to ASHRAE Standard 55 [27], acceptable thermal comfort conditions are defined by a *PMV* interval of −0.5 to +0.5, indicating that nearly all simulated cases satisfy the recommended comfort criteria. The vertical *PMV* profiles perfectly reflect the influence of temperature stratification within the occupied zone, which is consistent with the temperature distributions presented earlier in Figure 6. At lower heights near the ankle level (H = 0.1 m), *PMV* values tend to be negative, indicating a slightly cool thermal sensation caused by the supply of cooler air near the floor: a characteristic behavior of impinging jet ventilation systems operating in cooling mode. An exception to this trend is observed for the corner 2 configuration, where higher *PMV* values are recorded near the

floor, which is likely due to localized airflow interaction and reduced cooling effectiveness in that region. As the height increases, *PMV* values gradually rise and become positive, reflecting warmer thermal sensations near the upper occupied zone due to vertical thermal gradients. For more specific discussions, it is worth noting that, for all studied cases of corner 1 (colored by blue lines), the *PMV* reported values range from −0.32 to 0.1. As for the same location of corner 1, the circular geometry recorded the lowest value at the lower height levels (−0.32), while both circular and triangular geometries are competitive for the highest *PMV* value (+0.1) at higher height levels. Considering all cases of mid-wall 1 (colored by violet lines), the *PMV* reported values range from −0.12 to +0.1. As for the same location of mid-wall 1, the circular geometry recorded the lowest value at the lower height levels (−0.12), while the triangular geometry achieved the highest *PMV* value (+0.1) at higher height levels. The cases of mid-wall 2 (colored by orange lines) report *PMV* values between −0.1 and +0.2. As for the same location of mid-wall 2, the triangular geometry recorded the lowest value at the lower height levels (−0.1), while both the triangular and square geometries achieved the highest *PMV* value (+0.2) at higher height levels. The last cases of corner 2 (colored by red lines) report *PMV* values between +0.2 and +0.52, with the characterized inverted trend as described previously, which justified the possibility of its rejection among other studied locations. Generally, for the same location of corner 2, it can be observed that at lower height levels, the circular geometry yields lower *PMV* values compared to the other studied geometries, while all geometries exhibit nearly the same *PMV* value at higher height levels.

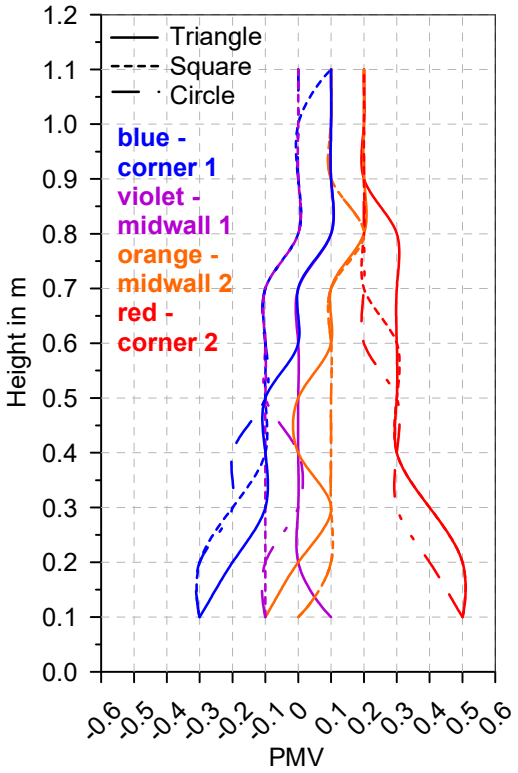

Figure 9. Variation in *PMV* with height in the local working zone (0.1–1.1 m above the floor) for all simulated cases.

Based on the preceding detailed discussions on *PMV* trends, it could be deduced that, among all configurations, the mid-wall 1 location consistently exhibits the *PMV* values closest to thermal neutrality (*PMV* ≈ 0) across most heights. This behavior indicates a more balanced thermal environment and reduced vertical discomfort, making this configuration more favorable compared to corners and other mid-wall placements. The improved *PMV*

distribution at this location can be attributed to more uniform airflow spreading and weaker stratification within the occupied zone.

Figure 10 presents the predicted percentage of dissatisfied (*PPD*) profiles corresponding to the *PMV* results. The majority of the evaluated cases demonstrate *PPD* values below 10%, which complies with the ASHRAE-recommended threshold for acceptable thermal comfort [37]. Such values indicate that a high proportion of occupants would experience satisfactory thermal conditions under the investigated scenarios. However, an increase in *PPD* is observed at lower heights (H $\leq$ 0.4 m) in several cases, corresponding to higher air velocities and cooler temperatures near the floor. This localized increase in dissatisfaction highlights the sensitivity of occupants to airflow conditions in the lower part of the occupied zone, particularly in displacement- and impingement-based ventilation strategies.

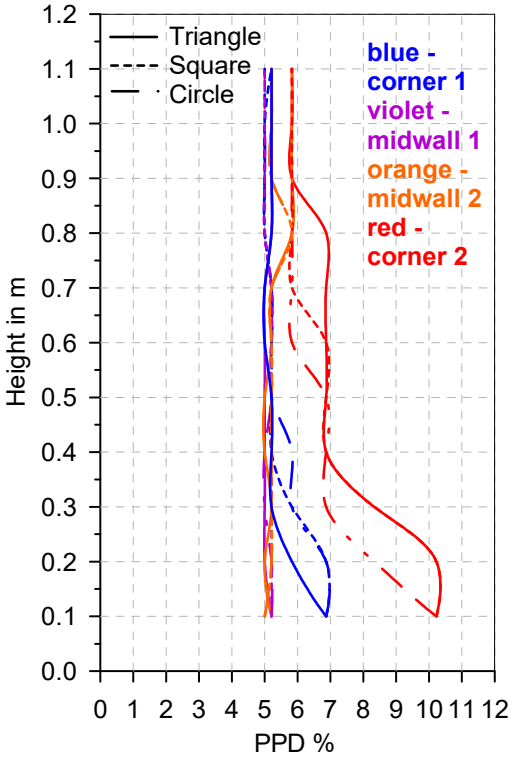

Figure 10. *PPD* as a function of height in the local working zone (0.1–1.1 m above the floor) for all simulated cases.

Overall, the combined *PMV* and *PPD* analyses confirm that impinging jet ventilation can provide acceptable thermal comfort within office environments, while also emphasizing the importance of diffuser placement and airflow distribution in minimizing local discomfort and enhancing occupant satisfaction.

4.2. Indoor Air Quality Based on Air Change Effectiveness

The air change effectiveness (*ACE*—Equation (6)) value at the head level (H = 1.1 m) for all instances examined is depicted in Figure 11. The ACE value findings are frequently found to be above the threshold of 1.0. This demonstrates the high efficiency of the *IJV* system in removing pollutants and providing fresh air at the head level. It is worth noting that studying the influence on other indoor air quality indices, such as contaminant transport, is an interesting area for future studies.

At the conclusion of this subsection, it can be noted that although all four investigated *IJV* installation locations and diffuser cross-sectional geometries demonstrate acceptable thermal performance within the occupied zone, their influence on overall

thermal comfort indices remains relatively limited, as all cases fall within the recommended comfort thresholds. Nevertheless, noticeable differences are observed in the vertical temperature stratification profiles, particularly among the various *IJV* locations. These variations in stratification behavior provide a key basis for discriminating between the tested configurations.

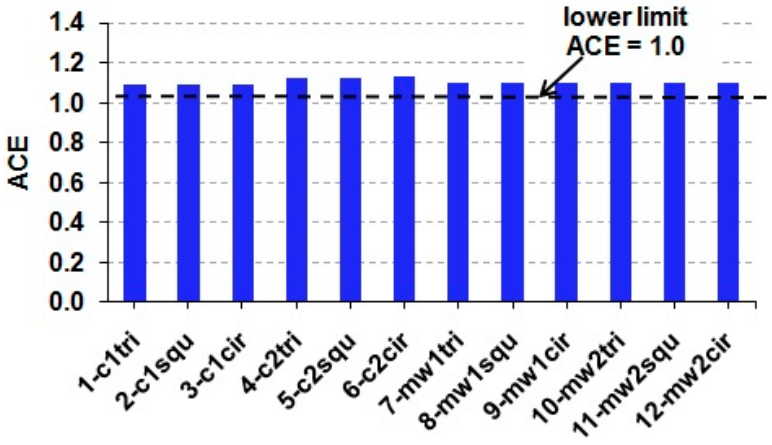

Figure 11. Air change effectiveness (*ACE*) for all studied simulations calculated at the head level (1.1 m above floor).

Specifically, the corner 2 configuration, located adjacent to the exterior hot wall, exhibits less favorable thermal characteristics and is therefore not recommended for practical application. In contrast, the mid-wall 1 configuration consistently yields lower *PMV* values and reduced vertical thermal gradients, indicating a more uniform and comfortable thermal environment within the working zone. Additionally, the results suggest that the circular diffuser cross-section offers improved thermal performance compared to the triangular and square geometries. Further insights into the suitability of each configuration are gained through a detailed analysis of airflow patterns and flow structures, which are discussed in the following section to inform the final selection of the optimal *IJV* location and geometry.

4.3. Flow Characteristics, Streamlines, and Temperature Contours

To study and compare the flow and temperature characteristics for different IJV cross-section geometrical shapes at the same *IJV* location, the three cases—triangle, square, and circle of corner 1 location as an example (simulations 1 to 3)—are selected here for presentation. Figure 12 shows the flow and temperature characteristics for the different geometries studied at the corner 1 location: (a) triangle, (b) square, and (c) circle, from left to right. On the left are isosurfaces of instantaneous vorticity ($\pm$0.07), colored by velocity magnitude; in the middle are streamlines at the room YZ midplane; and on the right are temperature contours at the room YZ midplane. The isosurfaces of instantaneous vorticity ($\pm$0.07) colored by velocity magnitude comparisons show comparable flow characteristics for the triangle and square cross sections. In contrast, limited enhanced flow characteristics are reported for the case of using the circular cross-section. This is also proven by comparing the streamlined photos at the room YZ midplane, where lower vortex intensity is observed for the use of a circle. At the same time, the temperature contours are found to be nearly identical for all cross sections used, as shown in the photos, confirming that the *IJV* cross-section shape has a lesser effect on the thermal stratifications. A similar conclusion is also found in previous research (Staveckis and Borodinecs [10]).

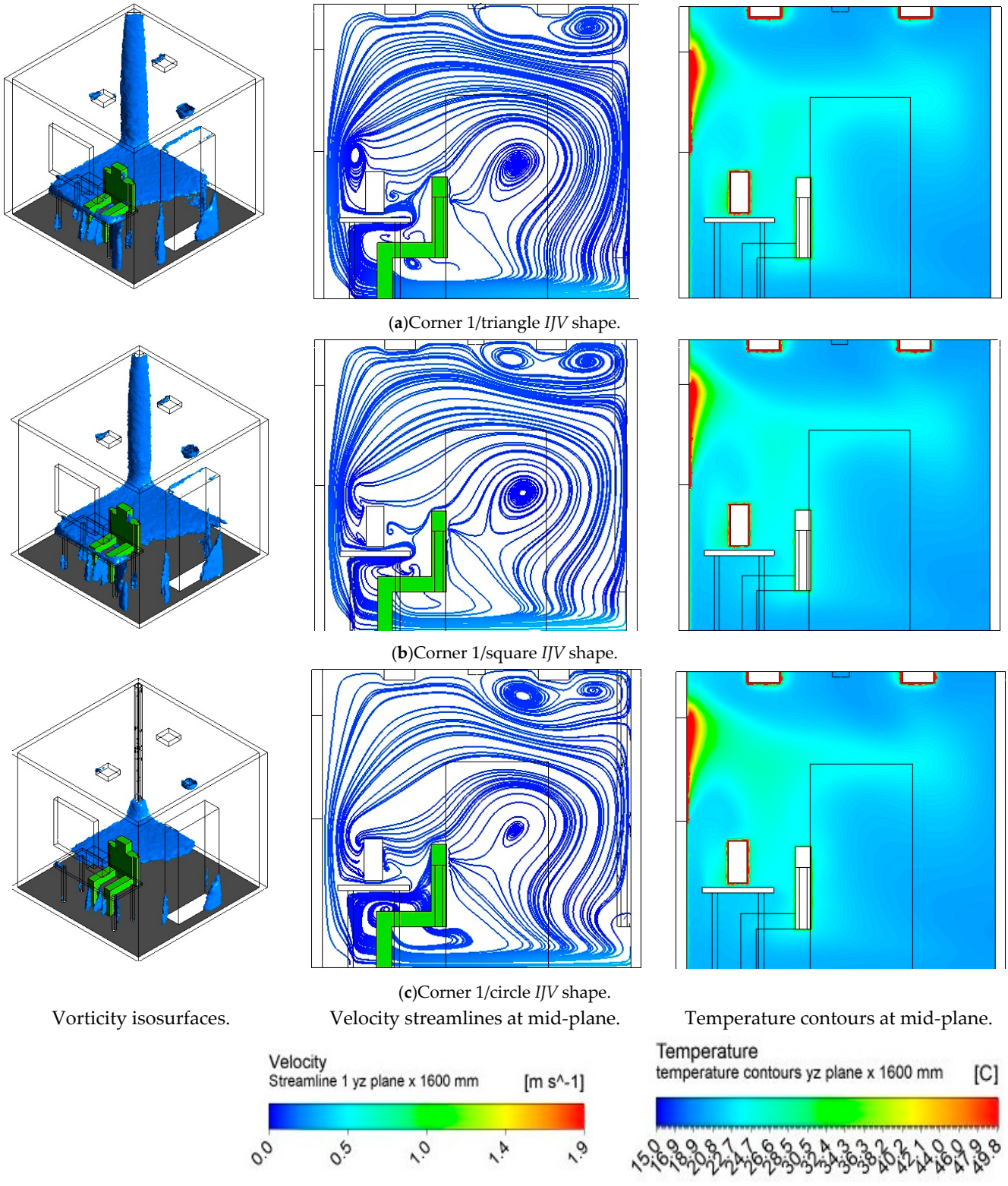

Figure 12. Flow and temperature characteristics for the cases of corner 1: (**a**) triangle, (**b**) square, and (**c**) circle. From **left** to **right**: On the **left** are isosurfaces of instantaneous vorticity (±0.07) colored by velocity magnitude, in the **middle** are velocity streamlines at room YZ mid-plane, and on the **right** are temperature contours at room YZ mid-plane.

To study and compare the flow and temperature characteristics of different *IJV* locations—namely corner 1, corner 2, mid-wall 1, and mid-wall 2—the best cross-section geometry, which is the round one, is selected for presentation here. Figure 13 shows flow

and temperature characteristics for only the circle cross-section geometry of different *IJV* locations—(a) corner 2, (b) mid-wall 2, and (c) mid-wall 1—while corner 1 can be observed from Figure 12c. From left to right: on the left are isosurfaces of instantaneous vorticity (±0.07), colored by velocity magnitude; in the middle are streamlines at the room YZ mid-plane; and on the right are temperature contours at the room YZ mid-plane. The results indicated the formation of a large vortex region behind the seated person for the case of the mid-wall 2 location (*IJV*, located in the mid-wall, right to the seated person). That can negatively affect the person's comfort inside the room. In contrast, the mid-wall location (*IJV* in the mid-wall behind the person and far from the hot exterior wall) reports significantly enhanced flow characteristics. The same conclusion for enhanced temperature stratification inside the local working zone is noted for the case of the mid-wall 1 location when comparing the temperature contour photos, while much higher temperatures are found at the ankle level inside the working zone for the case of the corner 2 location. This confirms the odd trend of temperature stratification, as observed previously in Figure 6. Similar trends are also found in a few works available in the literature, although with limited information [24]. Further supporting the aforementioned deduced information and discussion from Figures 12 and 13, Table 5 is presented to list the maximum vorticity swirl strength and averaged temperature values inside the working zone for all circular *IJV* cases, while the corner 2 location is excluded due to its rejection, as previously discussed. It can be found from Table 5 that the lowest vorticity swirl strength (0.09228 s^{-1}) was reported by the mid-wall 1 location compared to both locations of corner 1 and mid-wall 2 with the highest swirl value of 0.471722 s^{-1}. Also, it is clearly shown that the mid-wall 1 location verifies the lowest average temperature inside the working zone within acceptable comfort levels (21.81 °C) compared to the other locations of corner 1 and mid-wall 2. As a result, it is strongly suggested that the mid-wall 1 location is the best choice among other studied locations.

Table 5. Maximum vorticity swirl strength and averaged temperature inside the working zone for circular *IJV* cases.

Location	Max. Vorticity Swirl Strength (s^{-1})	Deviation (%)	Avg. Temperature (°C)	Deviation (%)
Mid-wall 2	0.471722	---	22.495	---
Corner 1	0.429991	−8.8465	22.774	1.2403
Mid-wall 1	0.309228	−34.447	21.814	−3.0273

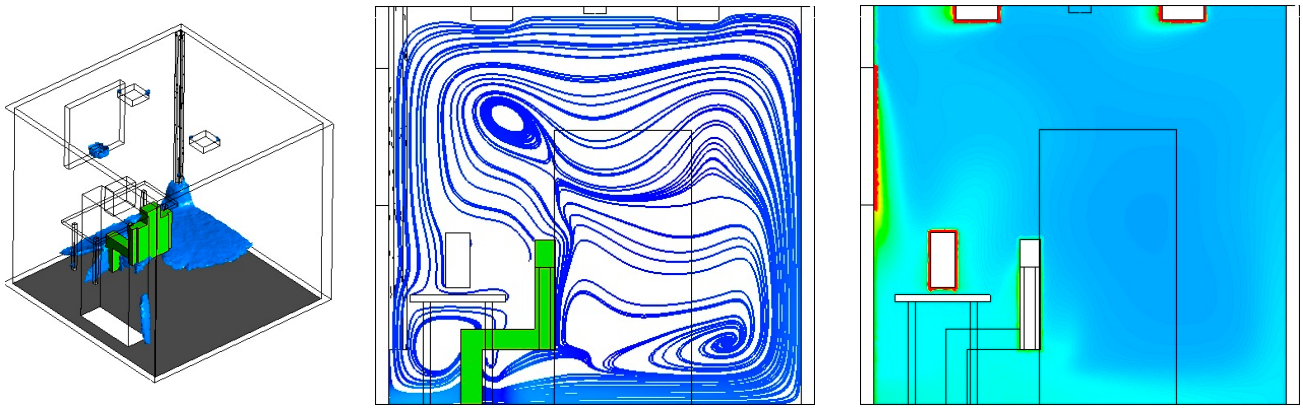

(**a**) Corner 2/circle *IJV* shape

Figure 13. *Cont.*

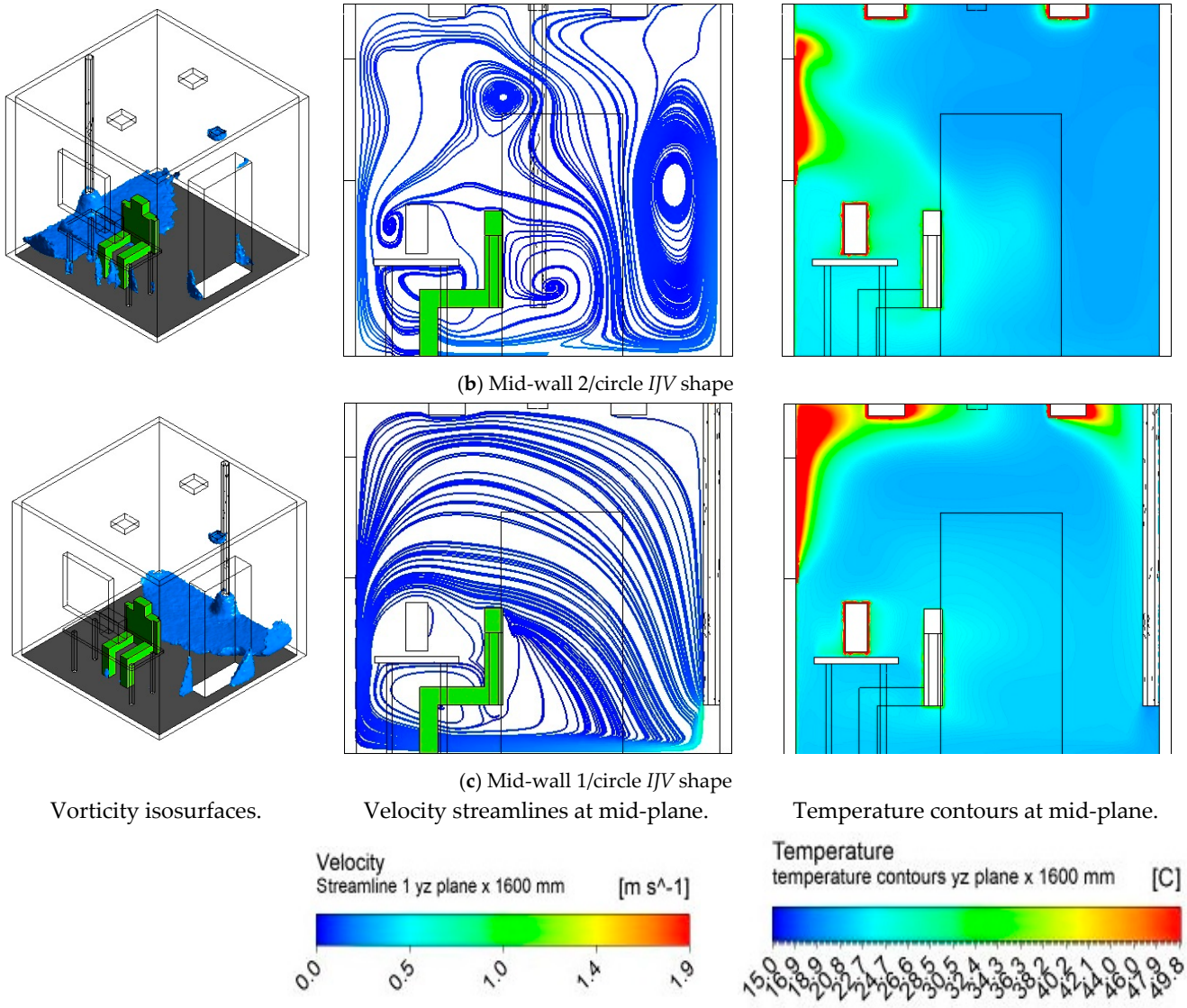

Figure 13. Flow and temperature characteristics for only circle cross section of different IJV locations: (**a**) corner 2, (**b**) mid-wall 1, and (**c**) mid-wall 2. From **left** to **right**: on the **left** are isosurfaces of instantaneous vorticity (±0.07) colored by velocity magnitude, in the **middle** are streamlines at room YZ mid-plane, and on the **right** are temperature contours at room YZ midplane.

5. Conclusions

In this work, comprehensive *CFD* simulations were conducted to investigate the impact of *IJV* diffuser geometry and installation location on airflow characteristics and thermal comfort performance. The simulations were carried out under cooling-mode conditions that were representative of a typical office environment in hot summer climates. The modeled space featured a seated thermal manikin and standard office furnishings, including a chair, desk, personal computer, and cupboard, with two ceiling-mounted lighting fixtures. The office contained one exterior wall with a 1 m^2 glazed window exposed to outdoor conditions of 38 °C and a solar radiation intensity of 700 W/m^2, while the remaining interior surfaces, including the floor and ceiling, were assumed to be adiabatic. The *IJV* air supply was installed at a height of 0.4 m, with constant inlet conditions of 20 °C supply air temperature, a flow rate of 75 m^3/h, and a relative humidity of 50%. A fully three-dimensional *CFD* model without symmetry assumptions was adopted, employing the RNG *k*–ε turbulence model with enhanced wall treatment. Four *IJV* installation positions were investigated to account for both functional performance and interior layout considerations:

two corner locations and two mid-wall locations, relative to a fixed occupant position, namely corner 1 (behind the manikin), corner 2 (in front of the manikin), mid-wall 1 (behind the manikin), and mid-wall 2 (to the right of the manikin). A combined return and exhaust outlet was located at the center of the ceiling, near the opposite wall. Additionally, three diffuser cross-sectional geometries with identical areas were analyzed, including a right triangular section ($163 \times 163 \times 230.5$ mm^3), a square section (115×115 mm^2), and a circular section (130.08 mm in diameter).

The results demonstrate that airflow patterns and temperature distributions are predominantly governed by the *IJV* installation location, rather than diffuser cross-section geometry. Among the tested geometries, the circular diffuser consistently exhibited improved airflow and thermal performance. Although all examined configurations met acceptable thermal comfort criteria, the mid-wall 1 position, located behind the occupant and away from the heated exterior wall, provided superior airflow distribution, reduced vortex formation, and lower temperature stratification within the occupied zone. It yielded the lowest vorticity swirl strength, with a deviation of about 34.5% lower than the highest value that was reported for the mid-wall 2 location. It also verified the lowest average temperature inside the working zone (21.8 °C), with a deviation of about 3% lower than the highest value that was reported for the mid-wall 2 location. Consequently, this configuration is recommended for similar office applications. These findings align well with the limited studies that are available in the literature and offer valuable insights for *HVAC* system designers.

Upcoming studies may extend this analysis to different room dimensions and occupant activity levels, investigating the influence on contaminant transport. From an architectural perspective, the superior performance of the mid-wall *IJV* configuration highlights the importance of incorporating ventilation strategies at the early stages of office design to support adaptable spatial layouts while maintaining thermal comfort.

Author Contributions: Conceptualization, M.A.K.; Methodology, M.A.K.; Software, M.A.K.; Validation, M.A.K.; Formal analysis, M.A.K.; Investigation, M.A.K.; Resources, N.A., A.M.A.A., A.F., H.A.R. and M.A.K.; Data curation, N.A., A.M.A.A., A.F., H.A.R. and M.A.K.; Writing—original draft, H.A.R. and M.A.K.; Writing—review & editing, H.A.R. and M.A.K.; Visualization, M.A.K.; Supervision, H.A.R. and M.A.K.; Project administration, H.A.R. and M.A.K.; Funding acquisition, N.A., A.M.A.A., A.F. and H.A.R. All authors have read and agreed to the published version of the manuscript.

Funding: This research received no external funding.

Data Availability Statement: The original contributions presented in the study are included in the article, further inquiries can be directed to the corresponding authors.

Conflicts of Interest: The authors declare no conflict of interest.

References

1. Karimipanah, T.; Awbi, H.B. Theoretical and experimental investigation of impinging jet ventilation and comparison with wall displacement ventilation. *Build. Environ.* **2002**, *37*, 1329–1342. [CrossRef]
2. Awbi, H.B. *Ventilation of Buildings*; Spon Press: London, UK, 2003.
3. Rohdin, P.; Moshfegh, B. Numerical predictions of indoor climate in large industrial premises. A comparison between different k-ε models supported by field measurements. *Build. Environ.* **2007**, *42*, 3872–3882.
4. Varodompun, J. Architectural and HVAC Applications of Impinging Jet Ventilation Using Full Scale and CFD Simulation. Ph.D. Thesis, University of Michigan, Ann Arbor, MI, USA, 2008.
5. Chen, H.J.; Moshfegh, B.; Cehlin, M. Investigation on the flow and thermal behavior of impinging jet ventilation systems in an office with different heat loads. *Build. Environ.* **2013**, *59*, 127–144. [CrossRef]
6. Yuan, X.X.; Chen, Q.Y.; Glicksman, L.R. A critical review of displacement ventilation. *ASHRAE Trans.* **1998**, *104*, 78–90.
7. Melikov, A.K.; Langkilde, G.; Derbiszewski, B. Airflow characteristics in the occupied zone of rooms with displacement ventilation. *ASHRAE Trans.* **1990**, *96*, 555–563.

8. Chen, H.J.; Moshfegh, B.; Cehlin, M. Numerical investigation of the flow behavior of an isothermal impinging jet in a room. *Build. Environ.* **2012**, *49*, 154–166. [CrossRef]
9. Varodompun, J.; Navvab, M. HVAC ventilation strategies: The contribution for thermal comfort, energy efficiency, and indoor air quality. *J. Green Build.* **2007**, *2*, 131–150. [CrossRef]
10. Staveckis, A.; Borodinecs, A. Impact of impinging jet ventilation on thermal comfort and indoor air quality in office buildings. *Energy Build.* **2021**, *235*, 110738. [CrossRef]
11. Hu, J.; Kang, Y.; Lu, Y.; Yu, J.; Li, H.; Zhong, K. Numerical investigation of the thermal and ventilation performance of a combined impinging jet ventilation and passive chilled beam system. *Build. Environ.* **2022**, *226*, 109726. [CrossRef]
12. Chen, H.; Moshfegh, B.; Cehlin, M. Computational investigation on the factors influencing thermal comfort for impinging jet ventilation. *Build. Environ.* **2013**, *66*, 29–41. [CrossRef]
13. Cehlin, M.; Karimipanah, T.; Larsson, U.; Ameen, A. Comparing thermal comfort and air quality performance of two active chilled beam systems in an open-plan office. *J. Build. Eng.* **2019**, *22*, 56–65. [CrossRef]
14. Zhang, P.; Djeddou, M.; Su, X.; Gao, G.; Lu, W. An impinging jet ventilation approach for automotive cabins: Promoting coughing droplet mitigation and thermal comfort enhancement. *Appl. Therm. Eng.* **2025**, *281*, 128696. [CrossRef]
15. Duan, T.; Ye, X.; Du, P.; Xi, W.; Kang, Y.; Zhong, K. Sinusoidal airflow modulation in impinging jet ventilation: Optimizing thermal comfort and energy efficiency through parametric analysis. *Energy Build.* **2026**, *350*, 116650.
16. Yakhot, V.; Orszag, S.A. Renormalization group analysis of turbulence. I. Basic Theory. *J. Sci. Comput.* **1986**, *1*, 3–51. [CrossRef]
17. Ye, X.; Kang, Y.; Yang, F.; Zhong, K. Comparison study of contaminant distribution and indoor air quality in large-height spaces between impinging jet and mixing ventilation systems in heating mode. *Build. Environ.* **2019**, *160*, 106159. [CrossRef]
18. Hu, J.; Kang, Y.; Yu, J.; Zhong, K. Numerical study on thermal stratification for impinging jet ventilation system in office buildings. *Build. Environ.* **2021**, *196*, 107798. [CrossRef]
19. Hu, J.; Kang, Y.; Lu, Y.; Yu, J.; Zhong, K. Simplified models for predicting thermal stratification in impinging jet ventilation rooms using multiple regression analysis. *Build. Environ.* **2021**, *206*, 108311. [CrossRef]
20. Ameen, A.; Cehlin, M.; Larsson, U.; Yamasawa, H.; Kobayashi, T. Numerical investigation of the flow behavior of an isothermal corner impinging jet for building ventilation. *Build. Environ.* **2022**, *223*, 109486. [CrossRef]
21. Ameen, A.; Cehlin, M.; Yamasawa, H.; Kobayashi, T.; Karimipanah, T. Energy saving, indoor thermal comfort and indoor air quality evaluation of an office environment using corner impinging jet ventilation. *Dev. Built Environ.* **2023**, *15*, 100179. [CrossRef]
22. Yang, B.; Liu, P.; Liu, Y.; Wang, F. Performance evaluation of ductless personalized ventilation combined with impinging jet ventilation. *Appl. Therm. Eng.* **2023**, *222*, 119915. [CrossRef]
23. Ameen, A.; Rashid, F.L.; Al-Obaidi, M.A.; Bouabidi, A.; Agyekum, E.B.; Chibani, A.; Kezzar, M. A review of impinging jet ventilation for indoor environment control. *Int. J. Thermofluids* **2025**, *29*, 101384. [CrossRef]
24. Yamasawa, H.; Kobayashi, T.; Yamanaka, T.; Choi, N.; Cehlin, M.; Ameen, A. Effect of supply velocity and heat generation density on cooling and ventilation effectiveness in room with impinging jet ventilation system. *Build. Environ.* **2021**, *205*, 108299. [CrossRef]
25. Almohammadi, B.A.; Hussein, E.; Almohammadi, K.M.; Refaey, H.A.; Karali, M.A. Energy Saving for Impinging Jet Ventilation System by Employing Various Supply Duct Locations and Return Grill Elevation. *Buildings* **2024**, *14*, 3716. [CrossRef]
26. Qin, C.; Lu, W. Effects of ceiling exhaust location on thermal comfort and age of air in room under impinging jet supply scheme. *J. Build. Eng.* **2021**, *35*, 101966. [CrossRef]
27. *ANSI/ASHRAE Standard 55-2020*; American Society of Heating and Refrigerating and Air-Conditioning Engineers, Thermal Environmental Conditions for Human Occupancy. AHSRAE Standard: Atlanta, GA, USA, 2021.
28. *ANSYS CFX-Solver Theory Guide*; R 18.0; ANSYS Inc.: Canonsburg, PA, USA, 2017.
29. Karali, M.A.; Almohammadi, B.A.; Mahfouz, A.S.; Abdelmohimen, M.A.H.; Attia, E.; Refaey, H.A. Effect of surfaces roughness of a staggered tube bank in cross flow with air on heat transfer and pressure drop. *Case Stud. Therm. Eng.* **2023**, *43*, 102779. [CrossRef]
30. Ameen, A.; Yamasawa, H.; Kobayashi, T. Numerical evaluation of the flow field of an isothermal dual-corner impinging jet for building ventilation. *Buildings* **2022**, *12*, 1767. [CrossRef]
31. Ameen, A.; Cehlin, M.; Larsson, U.; Karimipanah, T. Experimental investigation of the ventilation performance of different air distribution systems in an office environment—Cooling mode. *Energies* **2019**, *12*, 1354. [CrossRef]
32. *ISO 7730:2025*; Ergonomics of the Thermal Environment: Analytical Determination and Interpretation of Thermal Comfort Using Calculation of the PMV and PPD Indices and Local Thermal Comfort Criteria. ISO: Vernier, Switzerland, 2025.
33. Quadco Engineering PV Online Thermal Comfort Tool. Available online: https://www.quadco.engineering/en/know-how/cfd-calculate-pmv-and-ppd.htm (accessed on 23 March 2024).
34. Li, X.; Li, D.; Yang, X.; Yang, J. Total air age: An extension of the air age concept. *Build. Environ.* **2003**, *38*, 1263–1269. [CrossRef]
35. Ye, X.; Kang, Y.; Yan, Z.; Chen, B.; Zhong, K. Optimization study of return vent height for an impinging jet ventilation system with exhaust/return-split configuration by TOPSIS method. *Build. Environ.* **2020**, *177*, 106858. [CrossRef]

36. Fan, Y.; Li, X.; Yan, Y.; Tu, J. Overall performance evaluation of under floor air distribution system with different heights of return vents. *Energy Build.* **2017**, *147*, 176–187. [CrossRef]
37. *ANSI/ASHRAE Standard 129-1997*; Measuring Air-Change Effectiveness. AHSRAE Standard: Atlanta, GA, USA, 1997.